Facile Synthesis of The Li-Rich Layered Oxide $Li_{1.23}Ni_{0.09}Co_{0.12}Mn_{0.56}O_2$ with Superior Lithium Storage Performance and New Insights into Structural Transformation of the Layered Oxide Material during Charge−Discharge Cycle: In Situ XRD Characterization

Chong-Heng Shen, Qin Wang, Fang Fu, Ling Huang,* Zhou Lin, Shou-Yu Shen, Hang Su, Xiao-Mei Zheng, Bin-Bin Xu, Jun-Tao Li, and Shi-Gang Sun*

Department of Chemistry, College of Chemistry and Chemical Engineering, Xiamen University, Xiamen, Fujian 361005, China

Ⓢ Supporting Information

ABSTRACT: In this work, the Li-rich oxide $Li_{1.23}Ni_{0.09}Co_{0.12}Mn_{0.56}O_2$ was synthesized through a facile route called aqueous solution-evaporation route that is simple and without waste water. The as-prepared $Li_{1.23}Ni_{0.09}Co_{0.12}Mn_{0.56}O_2$ oxide was confirmed to be a layered $LiMO_2$–Li_2MnO_3 solid solution through ex situ X-ray diffraction (ex situ XRD) and transmission electron microscopy (TEM). Electrochemical results showed that the Li-rich oxide $Li_{1.23}Ni_{0.09}Co_{0.12}Mn_{0.56}O_2$ material can deliver a discharge capacity of 250.8 mAhg^{-1} in the 1st cycle at 0.1 C and capacity retention of 86.0% in 81 cycles. In situ X-ray diffraction technique (in situ XRD) and ex situ TEM were applied to study structural changes of the Li-rich oxide $Li_{1.23}Ni_{0.09}Co_{0.12}Mn_{0.56}O_2$ material during charge−discharge cycles. The study allowed observing experimentally, for the first time, the existence of β-MnO_2 phase that is appeared near 4.54 V in the first charge process, and a phase transformation of the β-MnO_2 to layered $Li_{0.9}MnO_2$ is occurred in the initial discharge process by evidence of in situ XRD patterns and selected area electron diffraction (SAED) patterns at different states of the initial charge and discharge process. The results illustrated also that the variation of the in situ X-ray reflections during charge−discharge cycling are clearly related to the changes of lattice parameters of the as-prepared Li-rich oxide during the charge−discharge cycles.

KEYWORDS: Li-rich layered oxide, aqueous solution evaporation, in situ XRD, β-MnO_2, layered $Li_{0.9}MnO_2$
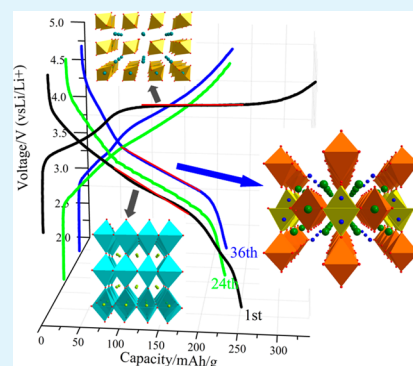
1. INTRODUCTION

Although the layered oxide $LiMO_2$ (M = Co, Mn, Ni) cathode of lithium ion battery has been investigated extensively by researchers, it is unable to match the demand on energy of electric vehicles (EVs) becaue of its limited capacity and power density.[1] Recently, the Li-rich layered oxide (zLi_2MnO_3·$(1-z)LiMO_2$), which are solid solutions between layers of Li_2MnO_3 and $LiMO_2$ (M = Mn, Ni, and Co), have become attractive because they exhibit high capacities of ~250 mAhg^{-1} when charged above 4.5 V.[2] As illustrated in Figure 1, both Li_2MnO_3 and $LiMO_2$ are layered materials, they belong to different groups in terms of the ion ordering in cell. The former belongs to the $C2/m$ group and monoclinic structural crystal system, while the latter associates to rhombohedral crystal system. Li-rich layered oxide cathode has no difference with $LiMO_2$ in electrochemical behaviors below 4.50 V. However, the Li_2MnO_3 is activated at 4.50 V in 1st charge where lithium ions extract from Li$^+$ layers with vacancies of O^{2-}, which results in layered MnO_2 component and followed by a lowering of the oxidation state of the transition metal(TM) ions in the subsequent discharges compared to that in the initial material.[3] The high capacity is attributed to the irreversible loss of O^{2-} from the lattice with the help of this reaction.[4] However,

the yielded oxygen gas evolution would cause critical safety problems. In addition, this material is susceptible to leaching out transition metal ions during high voltage cycling, especially at elevated temperatures, which leads to significant degradation of cycle performance.[5] What's more, this material has a low coulombic efficiency at the 1st cycle, poor rate capability and voltage fade during discharge process.[1] The voltage fade has become a serious problem to keep the Li-rich layered oxide materials from practical use.

To improve the electrochemical performance of the Li-rich layered oxide materials, it is essential to explore details of structural changes and phase transformation at different states. In situ X-ray diffraction is a useful technique to monitor the structural changes by real time.[6] Previously, $LiCoO_2$, $LiNiO_2$, Li_2MnO_4, and $LiNi_{1/3}Co_{1/3}Mn_{1/3}O_2$ oxides have been investigated by Yang and co-workers.[7−10] Liao et al. have reported that the $Li_{1-x}Ni_{0.5}Co_{0.25}Mn_{0.25}O_2$ and $LiNi_{0.6-x}Mg_xCo_{0.25}Mn_{0.15}O_2$ have tendency of transforming into spinel phase.[7−14] Ohsawa et al. illustrated the SAEDs of $Li[Ni_{0.17}Li_{0.2}Co_{0.07}Mn_{0.56}]O_2$,
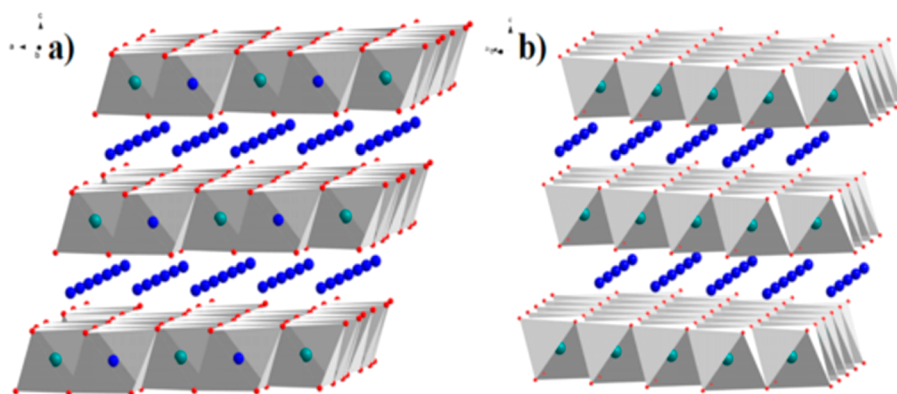
Figure 1. Structure of Li_2MnO_3 and $LiMO_2$ (a, b) Dark green, blue, and red spheres represent transition metal atoms, Li atoms, and O atoms, respectively.

and suggested that the spinel structure may form with the company of the initial electrochemical activation of Li_2MnO_3.[15] Mohanty et al. used in situ XRD technique to investigate $Li_{1.2}Co_{0.1}Mn_{0.55}Ni_{0.15}O_2$ electrode and found that the characteristic (440) peak of cubic crystal system appeared at 16th discharge, indicating the formation of spinel phase.[1] According to Loïc Simonin,[16] a new phase is created at the plateau potential of 4.50 V in the charge process of first cycle which has a close link to the starting phase and could be an oxygen deficient spinel. Despite above investigations, it is of urgent importance to further investigate at which conditions the spinel phase appears and the origin of this spinel phase formation, to have a better understanding of the structural changes in charge/discharge cycles of the materials. Furthermore, the electrochemical performances of Li-rich layered oxides materials effectively depend strongly on their structure and morphology. Many methods have been used recently to synthesize $xLi_2MnO_3 \cdot (1-x)LiMO_2$ materials and control their morphology, such as co-precipitation, combustion method, solid-state reaction at low temperature and sol–gel.[4,17−21] To the best of our knowledge the aqueous solution-evaporation route, which has advantage of simple and environment-friendly, is seldom reported.

The "voltage fade" in subsequent cycles was considered to be consequence of the formation of spinel phase. However, a series of problems such as how the phase transformation occurred in the solid solution cathode materials, which remained uncertain, have been challenging difficulties. No research reports have been found to focus on the forming process of spinel phase in layered Li-rich materials in electrochemical cycles though corresponding in situ XRD technique has been applied widely.

In this text, we captured the information on appearing of the β-MnO_2 phase for the first time, and traced the process of its transformation into layered $Li_{0.9}MnO_2$ in situation through in situ XRD and SAED patterns at different states of the initial cycle carefully. It is confirmed that the layered $Li_{0.9}MnO_2$ will transform into spinel phase in subsequent cycles by further TEM results. Our research revealed the key step and mechanism to the voltage fade in layered $Li_{1.23}Ni_{0.09}Co_{0.12}Mn_{0.56}O_2$ material, which could be instructive and meaningful to inhibit the voltage fade of layered Li-rich materials and improve cycle performances.

2. EXPERIMENTAL SECTION

2.1. Preparation of the Li-Rich Layer Oxide $Li_{1.23}Ni_{0.09}$-$Co_{0.12}Mn_{0.56}O_2$ Material. The precursor of $Li_{1.23}Ni_{0.09}Co_{0.12}Mn_{0.56}O_2$

was synthesized by means of aqueous solution evaporation route, which was prepared through addition of solution A into another one called solution B. First, 1 M solution A was prepared by mixing LiAc·$2H_2O$ with $Mn(Ac)_2 \cdot 4H_2O$ with stoichiometric mole ratio of Li/Mn = 2:1, and the 1 M solution B contains LiAc·$2H_2O$, $Ni(Ac)_2 \cdot 2H_2O$, $Co(Ac)_2 \cdot 2H_2O$, and $Mn(Ac)_2 \cdot 4H_2O$ with ratio of Li/Ni/Co/Mn = 1:0.292:0.375:0.333. Both solutions A and B were stirred for 6 h at room temperature. Then, solution B was placed in water bath at 80 °C with dropwise addition of solution A, and then the mixture was evaporated continually until it turned into brown bubble film. Finally, the precursor was achieved by burning the film in the hot plate at 300 °C. $Li_{1.23}Ni_{0.09}Co_{0.12}Mn_{0.56}O_2$ was achieved by successively heating of the precursor in air at 900 °C for 12 h, the product was then quenched.

2.2. Electrochemical Charge–Discharge Tests of $Li_{1.23}Ni_{0.09}Co_{0.12}Mn_{0.56}O_2$ Electrode. The cathode was prepared by casting the slurry consisting of 80 wt % active material ($Li_{1.23}Ni_{0.09}$-$Co_{0.12}Mn_{0.56}O_2$), 10 wt % acetylene black and 10 wt % polyvinylidene fluoride(PVDF) binder dissolving in N-methy pyrrolidone (NMP) onto aluminum foil and dried at 120 °C overnight. The Electrochemical performances of the prepared cathode were characterized in a 2025 coin type cell, which was assembled in an agron-filled glovebox. The cathode is separated from a lithium metal disk by a piece of Celgard separator. 1 M LiPF6 in 3:7 EC/DMC (volume) solution was employed as the electrolyte. The cells were tested at 0.1C (1 C = 250 mA/g) between 4.8 and 2.0 V at 25 °C by using CT2001 Land battery tester.

2.3. Structural Analysis of $Li_{1.23}Ni_{0.09}Co_{0.12}Mn_{0.56}O_2$ Material. The structure of the product was characterized by X-ray diffraction on the Rigaku Ultima IV powder diffractometer with Cu Kα radiation (λ = 1.5418 Å). Hitachi S4800 SEM operated at 10 kV was used to characterize the morphology of the as-prepared material. HRTEM test was conducted in JEM2100 at accelerating voltage of 200 kV.

The in situ XRD cell device consisted of a copper-made base and an upper cover with a sealed Kapton film allowing penetration of the X-rays through and an electrode plate soaked in Electrolyte. The data was collected in Rigaku Ultima IV powder diffractometer with operating voltage 40 kV and current 25 mA. Cu Kα (λ = 1.5418 Å) was used as source and a scan rate of 1 deg/min. The charge/discharge test was carried out under condition of 0.06 C for the initial charge and 0.25 C for the initial discharge process, respectively.

3. RESULTS AND DISCUSSION

3.1. Characterization of $Li_{1.23}Ni_{0.09}Co_{0.12}Mn_{0.56}O_2$ Material and Its Electrochemical Performances. *3.1.1. Structural Analysis of $Li_{1.23}Ni_{0.09}Co_{0.12}Mn_{0.56}O_2$ Material.* Figure 2a shows the ex situ XRD pattern of $Li_{1.23}Ni_{0.09}Co_{0.12}Mn_{0.56}O_2$. The strong peaks can be indexed by α-$NaFeO_2$ rock structure belonging to $R\bar{3}m$ group symmetry, and the three weak peaks at 20.7°, 21.7°, and 24.2° can be indexed by (020), (110), and
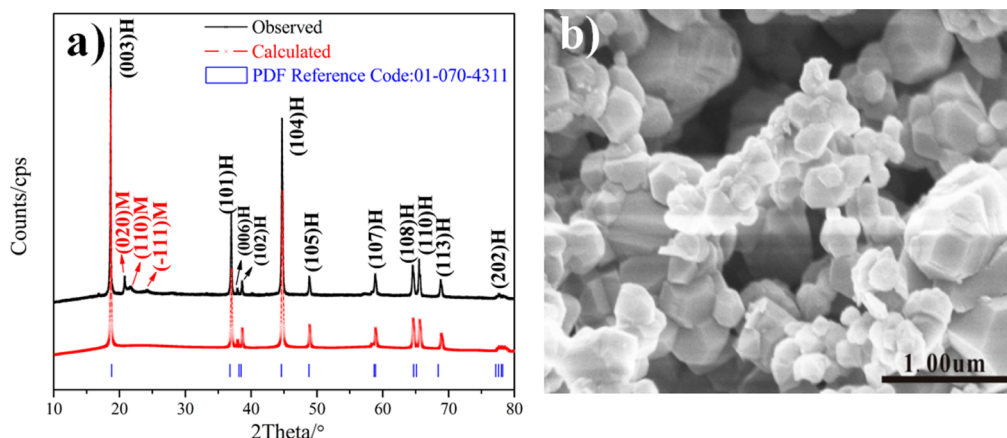
Figure 2. XRD pattern (a) and SEM image (b) of $Li_{1.23}Ni_{0.09}Co_{0.12}Mn_{0.56}O_2$.
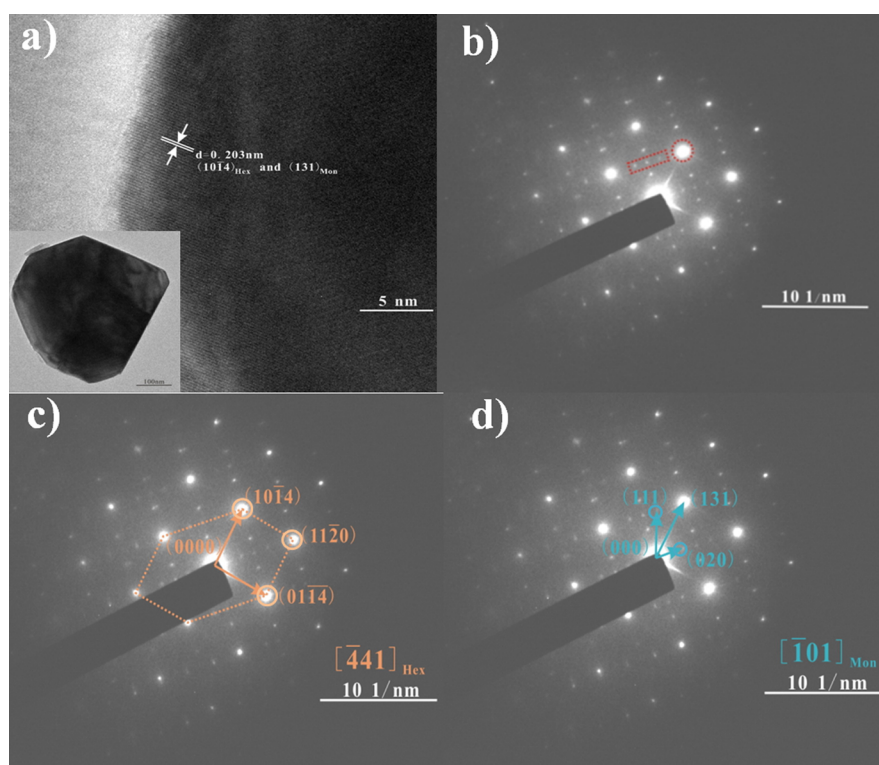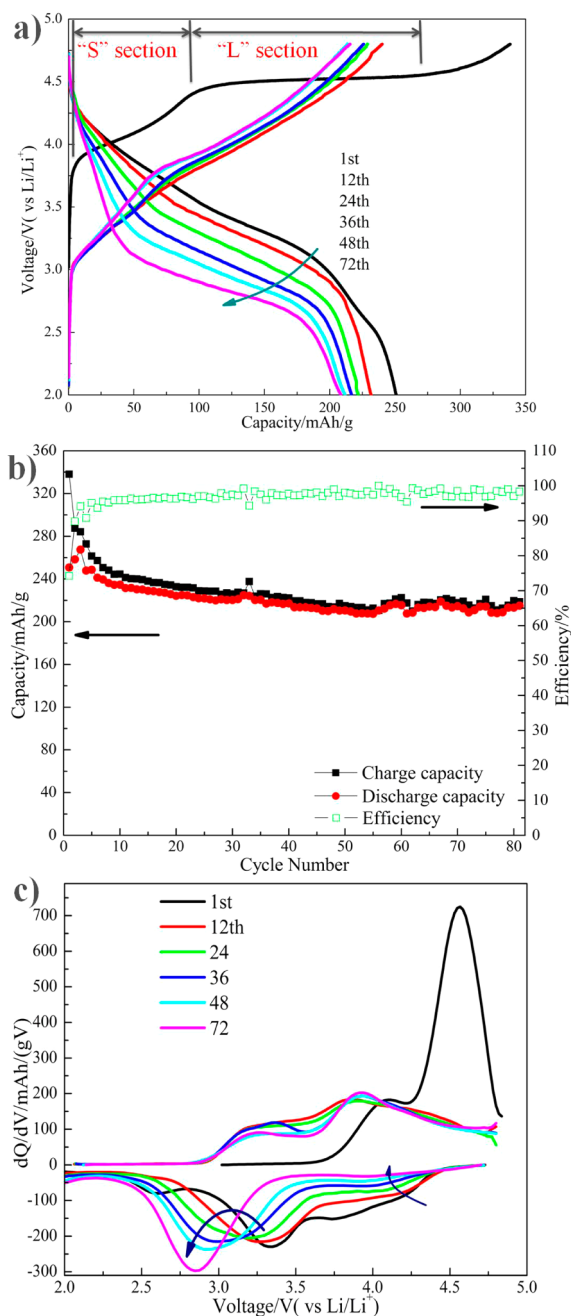

Figure 3. (a) High resolution transmission electron micrograph and (b) SAED pattern along zone axis and corresponding indexing SAED patterns (c, d) of $Li_{1.23}Ni_{0.09}Co_{0.12}Mn_{0.56}O_2$ particle. Inset is TEM of single $Li_{1.23}Ni_{0.09}Co_{0.12}Mn_{0.56}O_2$ particle.

($\bar{1}11$) diffractions of Li_2MnO_3.[2] The Li_2MnO_3 belongs to the monoclinic crystal system with C2/m group symmetry, and each LiO_6 octahedral interstice is surrounded by six MnO_6 octahedra making a hexagonal $LiMn_6$ neighbour unit in its Mn-rich layer.[2] The above analysis confirmed that the as-prepared $Li_{1.23}Ni_{0.09}Co_{0.12}Mn_{0.56}O_2$ material is a solid solution which is based on α-$NaFeO_2$ layered structure with monoclinic Li_2MnO_3.[1]

From Figure 2b, we can find that the particle of the product is a kind of polygonal prism with uniform distribution and good crystallinity. The average particle diameter of the product is about 400 nm.

The cell parameters of the product were refined by GSAS (R_{wp} = 0.0420, R_p = 0.0250, R_{F2} = 0.2627) as c = 14.215(3)Å, a = 2.843(1)Å, and V = 99.51 Å^3. The calculated ratio of cation disordering between Li^+ and Ni^{2+} is 2.16%, which indicates a

ordered arrangement between lithium ions and TM ions. The ratio of c/a is 5.000, which is greater than 4.899 for ideal cubic close stacking, suggesting the clear layered trait. The (006)/(102) and (108)/(110) doublets are sharp and splitted clearly, confirming the complete layered structure of the as-prepared $Li_{1.23}Ni_{0.09}Co_{0.12}Mn_{0.56}O_2$ material. In addition, cation disordering can also be measured by the ratio of intensity of (003) and (104) diffraction peaks,[4] the greater it is, the less the disordering is. It is generally concluded that the intact layered structure can form when the ratio is greater than 1.20. The ratio of I_{003}/I_{104} of the as-prepared $Li_{1.23}Ni_{0.09}Co_{0.12}Mn_{0.56}O_2$ material reaches 1.51 indicating that the level of cation disordering is quite low. R value ($R = [I_{(102)} + I_{(006)}]/I_{(101)}$) is a key factor to represent the hexagonal ordering, the lower it is, the more ordered the structure is. R value of the product is measured at 0.23, signifying that TM layers and Li^+ layers are sorted and ordered.[2]

Figure 4. (a) Charge and discharge curve in different cycles of, (b) cycle performance, and (c) differential capacity curve in different cycles of $Li_{1.23}Ni_{0.09}Co_{0.12}Mn_{0.56}O_2$.

A high resolution transmission electron micrograph of as-synthesized $Li_{1.23}Ni_{0.09}Co_{0.12}Mn_{0.56}O_2$ material is shown in Figure 3a, from which the distance between two lattice fringes is measured to be 0.203 nm corresponding to $(10\bar{1}4)_{Hex}$ of $LiMO_2$ and $(131)_{Mon}$ of Li_2MnO_3. The polygonal particle size can be measured about 400 nm from the inset. The selected area electron diffraction (SAED) along the zone axis in Figure 3b consists of two sets of reflections: parallelogram composed of neighbouring four bright spots and orthogonal triplet dark spots in the parallelogram. According to Mohanty et al.,[1] the existing of these triplet dark spots indicates the presence of Li_2MnO_3-like domains and the ordering of lithium ions with TM ions in TM layers. The pattern of spots marked by orange circle is for the layered $LiMO_2$ phase shown in Figure 3c and the pattern of spots marked by aqua green circle is for the monoclinic Li_2MnO_3 phase shown in Figure 3d. The triplet dark spots can also be found in another SAED patterns along zone axis and high resolution transmission electron micrograph in which $(0003)_{Hex}$ and $(001)_{Mon}$ planes may coexist and overlap of another particle of $Li_{1.23}Ni_{0.09}Co_{0.12}Mn_{0.56}O_2$ material (Supporting Information Figure S1).

In a word, the above results have confirmed the $LiMO_2$–Li_2MnO_3 solid solution did exist, and indicated that Li_2MnO_3 and $LiMO_2$ have structural compatibility ignoring of interplanar spacing deviation lattice distortion. In the $LiMO_2$–Li_2MnO_3 solid solution the $LiMO_2$ and Li_2MnO_3 could coexist along different crystal orientation and share the same lattice.

3.1.2. Electrochemical Performances of $Li_{1.23}Ni_{0.09}Co_{0.12}Mn_{0.56}O_2$ Material. Figure 4a shows charge and discharge curves of $Li_{1.23}Ni_{0.09}Co_{0.12}Mn_{0.56}O_2$ in different cycles. It is clear that the charge curve during the 1st cycle can be decomposed to two segments: (1) "S" section that ranges from 2.50 to 4.50 V, including reactions of $Ni^{2+} \rightarrow Ni^{3+}/Ni^{4+}$ or $Co^{3+} \rightarrow Co^{4+}$ and delithiation of $Li_{1.23}Ni_{0.09}Co_{0.12}Mn_{0.56}O_2$;[21] (2) "L" section that appears from 4.50 to 4.80 V, where Li_2MnO_3 was activated causing Li_2O stripping at 4.50 V platform and active MnO_2 provided much capacity with the appearance of O^{2-} vacancies leading to the irreversible capacity.[22] The discharge capacity of the electrode in the 1st cycle is 250.8 mAh/g with a coulombic efficiency of 74.2%. The irreversible capacity loss reaches to 87.3 mAh/g, and is attributed to lithium ions absence at sites in Li layers during lithium ions insertion because of O^{2-} vacancies appearing at charge platform of the 1st cycle. The electrode underwent a plateau potential stepping down in discharge process that was known as "voltage fade", which might be ascribed to the formation of the AB_2O_4 spinel-like structure during charge–discharge cycles.[1] The cycling performance curve of the $Li_{1.23}Ni_{0.09}Co_{0.12}Mn_{0.56}O_2$ material at 0.1 C is shown in
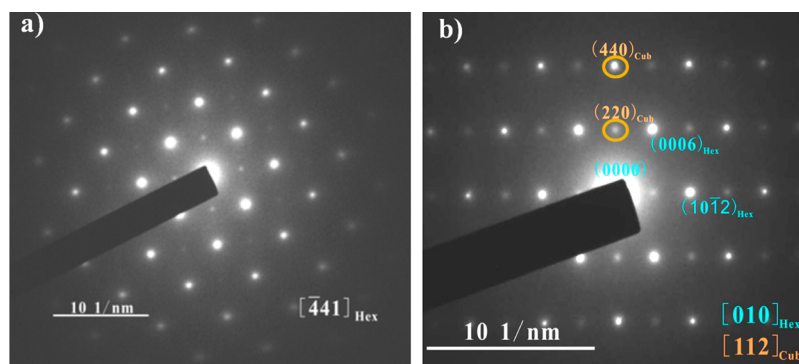
Figure 5. SAED patterns along $[\bar{4}41]_{Hex}$ and $[010]_{Hex}$ axis (a, b) of the $Li_{1.23}Ni_{0.09}Co_{0.12}Mn_{0.56}O_2$ after 36 charge–discharge cycles.

Figure 4b. The capacity retention of the electrode is 86.0% after 81 cycles. The capacity fade may be attributed to several factors: microstructure transformation during cycles, decomposition of electrolyte at high potential, and surface impedance.[1,3,19]

The dQ/dV plots of the charge/discharge curves in different cycles are illustrated in Figure 4c. The two dQ/dV peaks at 4.15 and 4.54 V in the 1st charge process are attributed to oxidation of $Ni^{2+} \rightarrow Ni^{3+}/Ni^{4+}$ and delithiating process of Li_2MnO_3. The oxidation of Co^{3+} to Co^{4+} might also occur partly between 4.15 and 4.54 V.[18,23] Ni^{4+} and Co^{4+} can be reduced at 3.42 and 3.75 V during the 1st discharge process, respectively.[24] After the activation of Li_2MnO_3 at 4.50 V in the 1st charge process, the redox pair of 4.15/3.75 V of 1st cycle has developed into a dominant redox pair of 3.93/2.85 V of in the 72nd cycle, suggesting that the local layered framework of $Li_{1.23}Ni_{0.09}Co_{0.12}Mn_{0.56}O_2$ has been transformed to spinel phase during cycles, which resulted in a layered-spinel intergrowth structure. It is notable that the redox peak at 4.20 V in the 12th cycle corresponds to extraction of lithium ions from tetrahedral sites of spinel-like domain. This phenomenon was ascribed to the complex cation ordering in the layered-spinel structural intergrowth face that leads the lithium ions extraction/insertion to escaping/filling of octahedral sites rather than tetrahedral sites. This transformation of layered structure to spinel is a tendency of electrode materials with high manganese content, especially $LiMnO_2$ and its derivatives.[25,26]

3.1.3. TEM Analysis of $Li_{1.23}Ni_{0.09}Co_{0.12}Mn_{0.56}O_2$ Materials after Charge−Discharge Cycling. Figure 5a shows a SAED pattern along the zone axis of $Li_{1.23}Ni_{0.09}Co_{0.12}Mn_{0.56}O_2$ material after 36th cycles of charge−discharge. It is clear that the triplet dark spots are almost disappear together with intensity of bright spots weakened, Such variation indicates that the Li_2MnO_3 component was completely consumed in subsequent cycles and the whole framework has been changed into layered α-NaFeO_2 structure with cubic close stacking between lithium ions and TM ions.

The spots marked by yellow ellipse in Figure 5 were from cubic spinel-like AB_2O_4, indicating that the local domain of the structure was changing.

3.2. In Situ XRD and Ex-TEM Investigation of $Li_{1.23}Ni_{0.09}Co_{0.12}Mn_{0.56}O_2$ Electrode during Charge−Discharge Cycling. *3.2.1. New Phase β-MnO_2 and Its Transformation.* As shown in Figure 6b, at the condition of charge rate at 0.06C and discharge rate at 0.25C, the diffraction peak marked in black elliptical frame in Figure 6a, appearing at about 40.75° in the charge process of 1st cycle, could be ascribed to (200) reflection of tetragonal β-MnO_2 (JCPDS No.12-0716). This new diffraction peak is kept shifting toward higher 2θ values until the end of the initial charge process. When the reflection peak reached at near 40.82° corresponding to the red rectangular area in Figure 6a, it could be assigned to (211) reflection of layered $Li_{0.9}MnO_2$ belonging to the orthorhombic crystal system with Pnma space group symmetry (JCPDS No.44-0144). Evidence of existence of tetragonal β-MnO_2 and orthorhombic $Li_{0.9}MnO_2$ can be found in Figure 7a and 7b which are SAED images captured at 4.54 and 3.00 V of the initial charge and discharge process, respectively. As indicated in Figure 7a, at 4.54 V of the initial charge process the pattern of spots marked by dark green dashed circle is for the tetragonal beta-MnO_2, while at 3.00 V of the initial discharge process the pattern of spots marked by dark yellow dashed circle in Figure 7b could be assigned to the orthorhombic $Li_{0.9}MnO_2$ phase. The evidences from both in situ XRD patterns and SAED
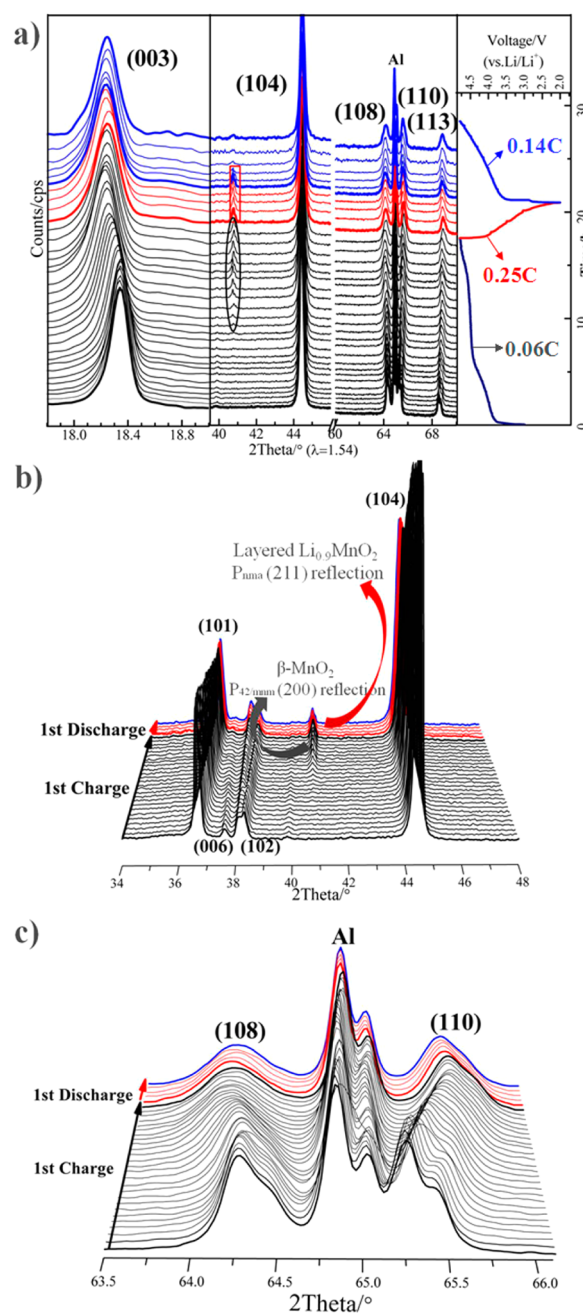
Figure 6. (a) General in situ XRD patterns of $Li_{1.23}Ni_{0.09}Co_{0.12}Mn_{0.56}O_2$ material in the first 1.5 cycles and (b, c) detail patterns of (101), (006), (102), (104), (108), and (110) reflections in the 1st cycle.

images taken by ex-TEM measurement demonstrate clearly the transformation of the beta-MnO_2 into $Li_{0.9}MnO_2$ phase at different states in the first charge/discharge process.

From Figure 8a and 8b, those two structures have a similar arrangement of Li ions and Mn ions, both of them share the same octahedral sites surrounded by O atoms. β-MnO_2 might absorb Li^+ to form a $Li_{0.9}MnO_2$ during intercalation of lithium ions (Supporting Information Figure S2a). As Da Wang et al. have recently illustrated that, through first-principles calculations along with cluster expansion techniques and based on the thermal reduction during the intercalation of lithium ions into β-MnO_2, a structural evolution to Li_xMnO_2 ($0 \leq x \leq 1$) would occur.[28]
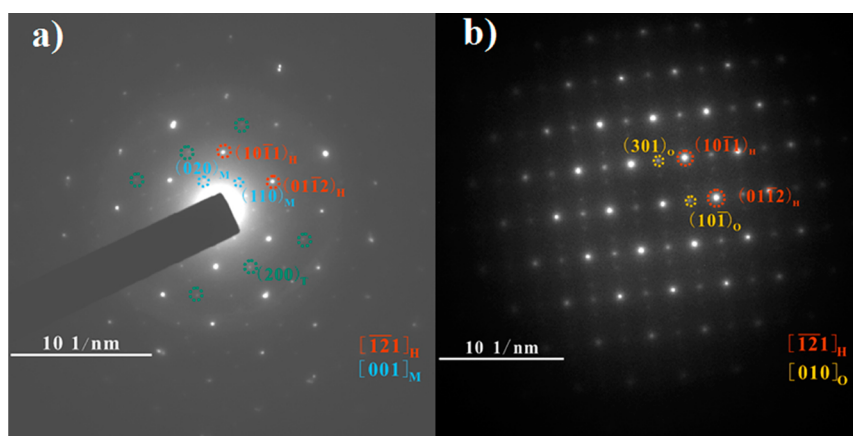
5520

dx.doi.org/10.1021/am405844b | *ACS Appl. Mater. Interfaces* 2014, 6, 5516−5524

Figure 7. SAED patterns of $Li_{1.23}Ni_{0.09}Co_{0.12}Mn_{0.56}O_2$ material at 4.54 V (a) and 3.00 V (b) of the initial charge and discharge process, respectively.
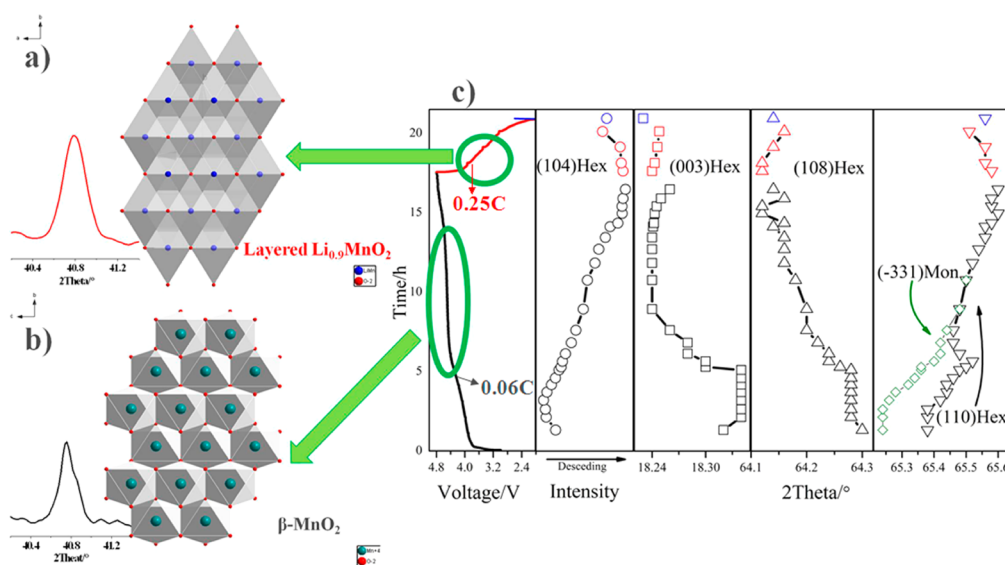

Figure 8. Structure of $Li_{0.9}MnO_2$ and β-MnO_2 (a, b) and trend of main reflections in the 1st cycle (c).

According to Armstrong et al.,[27] Mn ions in a layered LiMnO$_2$ can step through a common face into the vacant tetrahedral sites in Li$^+$ layers when there are enough Li vacancies. With the help of this displacement of Mn ions and the similar situation of Li$^+$ for which a lithium ion in the other neighbour layer migrates from an octahedral to the tetrahedral site that shares a face with the vacant Mn ion site, formation of a structure with this arrangement of an empty octahedral Mn ion site between tetrahedral Li and Mn ions, which was described as "dumbbell" is expected to happen (Supporting Information Figure S2b). This structure has been referred to as "splayered" and a further associated rearrangement of Li and Mn ions is thought to occur to form the spinel structure. Therefore, layered $Li_{0.9}MnO_2$ can easily transform to spinel structure during cycles. In addition, there was no sign of reflections of lithium oxide such as Li_2O that could be caused by insufficient accumulation. Moreover, we also find the width of (003) reflection is increasing during charge/discharge process, ascribing to crystal defects due to formation of the new phases.[11]

3.2.2. Variations of Main Reflections. As for (003) reflection shown in Figure 6a and Figure 8c, no shifting was observed during "S" section, while it shifts toward lower 2θ values obviously during the beginning of the "L" section, indicating that the c-axis starts stretching.[29] When the charge potential

reaches about 4.54 V, the (003) reflection begins to move to higher angle gradually. Meanwhile, the width of the (003) reflection starts to broaden. In the first discharge process, the (003) reflection starts shifting negatively. The c-parameter decreases at 2nd charge because the (003) reflection shifts positively. Also in the charge process of the 1st cycle, it can be found that, with the charging potential increasing, the (108) reflection and (110) reflection are separating clearly as shown in Figure 6c. The (108) reflection is moving to higher 2θ values and the (110) reflection is moving to lower 2θ values. This phenomenon demonstrates that the whole a-b plane in the charging process contracts first and subsequently it has a tendency to restore or expand gradually.[13]

No position variations were observed for the (101) and (104) reflections. However, variations are found in their intensities. Especially for (104) reflection in Figure 8c, it weakened in charge process and strengthened in discharge process. It is known that the weakening/strengthening in intensities of the (101) and (104) planes during charge/discharge cycle indicates the successful extraction/insertion of lithium ions.[1]

The disappearance of the (006) reflection and broadening of the (102) reflection at the end of charge process of the 1st cycle corresponds to a lowering tendency of R-value, meaning a distinguished layered trait. It could be found that the width and

intensities of the (108) and (110) reflections were broadening and weakening, respectively, illustrating that a lattice distortion was arising during the charge process of 1st cycle due to disordering of TM ions and lithium ions or O^{2-} vacancies.

3.2.3. Variations of Lattice Parameters and Layered Factors.

Figure 9a depicts a trend plots of $I_{(003)}/I_{(104)}$ and R-value of the
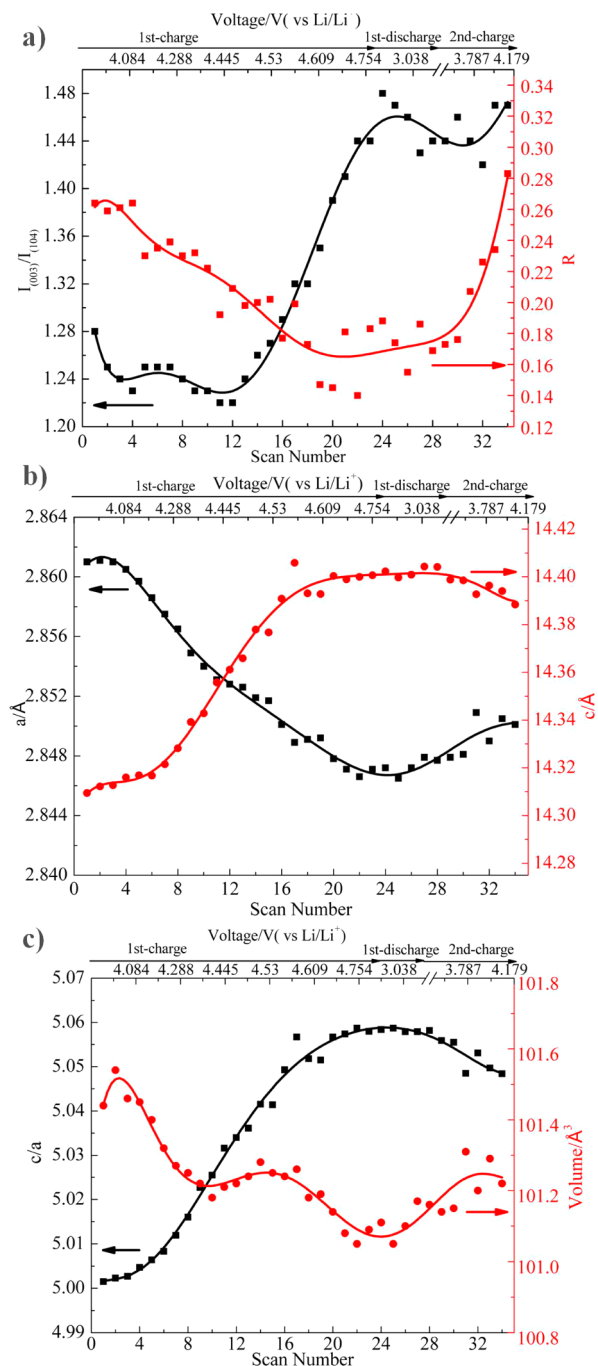
Figure 9. (a) Trend plots of $I_{(003)}/I_{(104)}$ and R-value of (b) the changes of lattice parameters of and (c) the changes of c/a and unit cell volume of Li$_{1.23}$Ni$_{0.09}$Co$_{0.12}$Mn$_{0.56}$O$_2$ during the first 1.5 cycles as a function of scan numbers.

as-synthesized Li$_{1.23}$Ni$_{0.09}$Co$_{0.12}$Mn$_{0.56}$O$_2$ material in the first 1.5 cycles. The ratio of $I_{(003)}/I_{(104)}$ is kept increasing while the R-value is decreased after 4.50 V in the charge process of 1st cycle, indicating that layered trait of the Li$_{1.23}$Ni$_{0.09}$Co$_{0.12}$Mn$_{0.56}$O$_2$

material was enhanced. Meanwhile, the formation of β-MnO$_2$ would occur at around 4.54 V when the monoclinic Li$_2$MnO$_3$ was activated. Since the spare lithium ions from Li−Mn rich zone of original Li$_2$MnO$_3$ were released, which would hinder the extraction of Li$^+$ caused by high diffusion energy barrier at high potential, some of those lithium ions disordered with Mn ions. The appearing of layered β-MnO$_2$ promotes and reinforces the whole layered characteristic. The R-value is upsurged during the charge process of 2nd cycle, on account of cations disordered arrangement caused by occupation of TM octahedral interstitial positions by lithium ions during insertion process. Figure 9b demonstrates a changing trend of c and a lattice parameters with potential. At the potential of about 4.10 V in the charge process of 1st cycle, TM ions started to be oxidized and lithium ions began extracting, which causes a-parameter decreasing sharply due to the decreasing of M−M distance caused by effective ionic radiation reducing (Ni^{2+}(0.69 Å) to Ni^{3+}(0.56 Å)/Ni^{4+}(0.48 Å) and Co^{3+}(0.61 Å) to Co^{4+}(0.53 Å)). In the voltage window of 4.45−4.54 V, in which the electrochemical activation of Li$_2$MnO$_3$ occurred and β-MnO$_2$ appeared, the extraction of lithium ions have deepened and led to a great reducing of the lithium shielding effect, which results in domination of the repulsion between O atoms, hence stretching the c-axis and increasing c-parameter.[2] When lithium ions disordered with Mn ions in the voltage window of 4.54−4.80 V, c and a parameters are kept stable attributed to the mutual inside-out of each layers between lithium ions and Mn ions. During the discharge process of 1st cycle, when the layered Li$_{0.9}$MnO$_2$ appeared, c-parameter rose again because the Li layers tended to be complete on account of insertion of lithium ions. Simultaneously, a-parameter increased due to the reduction of TM ions. During the charge process of 2nd cycle in potential range of 3.78−4.14 V, the TM ions occupied sites in the Li Layers, which led to c axis contracting. As a consequence the so c parameter began reducing.

The variations of c/a and cell volume during first 1.5 cycles are presented in Figure 9c. It is clear that the ratio of c/a reached a maximum value of 5.06 at potential of 4.54 V in the charge process of 1st cycle, indicating that layered structure turned to stretched vertically and contracted transversely. It could be found that the ratio of c/a maintained at 5.05 until the end of first 1.5 cycles and the cell volume stabilize at value of 101.0−101.4, which confirmed that the structure of Li$_{1.23}$Ni$_{0.09}$Co$_{0.12}$Mn$_{0.56}$O$_2$ material was not damaged.

An interpretive scheme for structural changes of the Li$_{1.23}$Ni$_{0.09}$Co$_{0.12}$Mn$_{0.56}$O$_2$ material during the 1st cycle is illustrated in Figure 10. The structure of as-synthesized Li$_{1.23}$Ni$_{0.09}$Co$_{0.12}$Mn$_{0.56}$O$_2$ was layered with arrangement of Li layers and TM layers alternately, and lithium ions occupied octahedral interstitial positions with a —ABC—ABC— close stacking. In voltage window of 4.10 to 4.40 V of the charge process of 1st cycle, the S section, Ni^{2+} or Co^{3+} was oxidized to Ni^{3+}/Ni^{4+} or Co^{4+}. The increasing repulsive forces between O atoms because of extraction of lithium ions associate with reducing of a-parameter and increasing of c-parameter. Hence, the ratio of c/a kept at a stable value, making crystal cell at a stretched state. In situ XRD results also indicated that the yielded dislocation or lattice distortion didn't affect stability of the body structure. Within potential range of 4.40−4.54 V in the charge process of 1st cycle, the L section, Li$_2$MnO$_3$ was activated and then consumed with extraction of lithium ions and appearance of O^{2-} vacancies, which caused sectional cation disordering and began forming a new phase β-MnO$_2$. Judging from the trend of $I_{(003)}/I_{(104)}$ in Figure 9a, we can speculate that the body
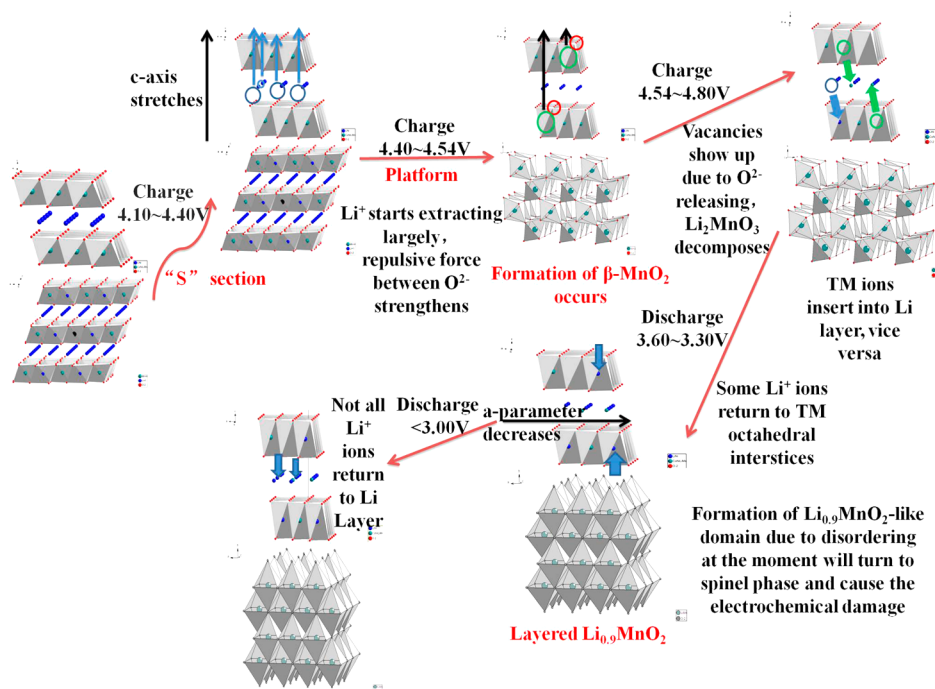
Figure 10. Interpretive scheme for structural changes of $Li_{1.23}Ni_{0.09}Co_{0.12}Mn_{0.56}O_2$ during 1st cycle.

structural integrity may be preserved owing to layered structure and ordered arrangement of β-MnO_2. In the voltage window of 4.54 to 4.80 V, c-parameter stopped increasing by reason for the fact that TM ions migrates into empty sites in Li layers which could weaken the repulsive force between O atoms. When the potential turned to range of 3.60−3.30 V in the discharge process of 1st cycle, parts of lithium ions inserted into the TM ions octahedral interstitial positions, causing formation of layered $Li_{0.9}MnO_2$ gradually and triggering a disordered cations arrangement. Simultaneously, the a parameter starts increasing because of the reduction of TM ions. The yielded $Li_{0.9}MnO_2$ could transform to spinel-like $LiMn_2O_4$ in subsequent cycles, resulting voltage fade. At below 3.00 V of discharge potential, plenty of lithium ions inserted into original sites, which would shield the repulsion between O atoms and make c parameter decrease.

4. CONCLUSIONS

In summary, the Li-rich layered $Li_{1.23}Ni_{0.09}Co_{0.12}Mn_{0.56}O_2$ material with superior lithium storage performance was successfully synthesized through aqueous solution-evaporation route. The ex situ XRD and TEM results demonstrated that the as-prepared Li-rich layered oxide was a layered superlattice solid solution including monoclinic Li_2MnO_3. The in situ XRD and SAED patterns at different states of the initial cycle results indicated a phase transformation from β-MnO_2 phase appearing beyond 4.54 V in the initial charge process to layered $Li_{0.9}MnO_2$ phase during the initial discharge process and a spinel phase formed after 24th cycle. Variations of the c and a parameters were actually related to the changes of repulsive forces between O atoms at octahedral positions during extraction/insertion and metal−metal distance depending on effective ionic radii. The layered $Li_{0.9}MnO_2$ phase could transform into splayered structural framework which is the key intermedium to spinel-like $LiMn_2O_4$, which is the key step to the voltage fade in subsequent electrochemical cycles. The structural evolution and microscopic self-adjustment such as variations of lattice parameters are directive and facilitated to improve cycle performances, inhibit voltage fade, and carry out effective elemental doping and coatings.

■ ASSOCIATED CONTENT

Ⓢ Supporting Information

High resolution transmission electron micrograph and SAED pattern along $[0\bar{1}0]_{Hex}$ zone axis and corresponding indexing of SAED patterns of another particle of $Li_{1.23}Ni_{0.09}Co_{0.12}Mn_{0.56}O_2$ material and phase transformation of β-MnO_2 into $Li_{0.9}MnO_2$ and splayered arrangement. This material is available free of charge via the Internet at http://pubs.acs.org.

■ AUTHOR INFORMATION

Corresponding Authors

*E-mail: huangl@xmu.edu.cn.
*E-mail: sgsun@xmu.edu.cn.

Notes

The authors declare no competing financial interest.

■ ACKNOWLEDGMENTS

■ REFERENCES

(1) Mohanty, D.; Kalnaus, S.; Meisner, R. A.; Rhodes, K. J.; Li, J. L.; Payzant, E. A.; Wood, D. L., III; Daniel, C. Structural Transformation of a Lithium-Rich $Li_{1.2}Co_{0.1}Mn_{0.55}Ni_{0.15}O_2$ Cathode during High Voltage Cycling Resolved by In Situ X-ray Diffraction. *J. Power Sources* **2013**, *229*, 239−248.

(2) Thackeray, M. M.; Kang, S. H.; Johnson, C. S.; Vaughey, J. T.; Benedek, R.; Hackney, S. A. Li_2MnO_3-Stabilized $LiMO_2$ (M = Mn, Ni, Co) Electrodes for Lithium-Ion Batteries. *J. Mater. Chem.* **2007**, *17*, 3112−3125.

(3) Wu, Y.; Manthiram, A. Effect of Surface Modifications on the Layered Solid Solution Cathodes $(1-z)$Li$[$Li$_{1/3}$Mn$_{2/3}]$O$_2-(z)$Li-$[$Mn$_{0.5-y}$Ni$_{0.5-y}$Co$_{2y}]$O$_2$. *Solid State Ionics* **2009**, *180*, 50−56.

(4) Du, K.; Zhou, W. Y.; Hu, G. R.; Peng, Z. D.; Jiang, Q. L. Synthesis and Electrochemical Properties of Li$[$Li$_{0.2}$Mn$_{0.54}$Ni$_{0.13}$Co$_{0.13}]$O$_2$ as Cathode Material for Li-Ion Batteries. *Acta Chim. Sin. (Engl. Ed.)* **2010**, *68*, 1391−1398.

(5) Park, M. S.; Lee, J. W.; Choi, W. C.; Im, D. M.; Doo, S. G.; Park, K. S. On the Surface Modifications of High-Voltage Oxide Cathodes for Lithium-ion Batteries: New Insight and Significant Safety Improvement. *J. Mater. Chem.* **2010**, *20*, 7208−7213.

(6) Richard, M. N.; Koetschau, I.; Dahn, J. R. A Cell for In Situ X-Ray Diffraction Based on Coin Cell Hardware and Bellcore Plastic Electrode Technology. *J. Electrochem. Soc.* **1997**, *144*, 554−557.

(7) Yang, X. Q.; Sun, X.; McBreen, J. New Findings on the Phase Transitions in Li$_{1-x}$NiO2: In situ Synchrotron X-ray Diffraction Studies. *Electrochem. Commun.* **1999**, *1*, 227−232.

(8) Yang, X. Q.; Sun, X.; McBreen, J. Structural Changes and Thermal Stability: In situ X-ray Diffraction Studies of a New Cathode Material LiMg$_{0.125}$Ti$_{0.125}$Ni$_{0.75}$O$_2$. *Electrochem. Commun.* **2000**, *2*, 733−737.

(9) Yang, X. Q.; Sun, X.; McBreen, J. New Phases and Phase Transitions Observed in Li$_{1-x}$CoO$_2$ During Charge: In situ Synchrotron X-ray Diffraction Studies. *Electrochem. Commun.* **2000**, *2*, 100−103.

(10) Yang, X. Q.; McBreen, J.; Yoon, W. S.; Grey, C. P. Crystal Structure Changes of LiMn$_{0.5}$Ni$_{0.5}$O$_2$ Cathode Materials during Charge and Discharge Studied by Synchrotron based In situ XRD. *Electrochem. Commun.* **2002**, *4*, 649−654.

(11) Liao, P. Y.; Duh, J. G.; Lee, J. F.; Sheu, H. S. Structural Investigation of Li$_{1-x}$Ni$_{0.5}$Co$_{0.25}$Mn$_{0.25}$O$_2$ by In situ XAS and XRD Measurements. *Electrochim. Acta* **2007**, *53*, 1850−1857.

(12) Liao, P. Y.; Duh, J. G.; Sheu, H. S. Structural and Thermal Properties of LiNi$_{0.6-x}$Mg$_x$Co$_{0.25}$Mn$_{0.15}$O$_2$ Cathode Materials. *J. Power Sources* **2008**, *183*, 766−770.

(13) Nam, K. W.; Yoon, W. S.; Shin, H. J.; Chung, K. Y.; Choi, S. D.; Yang, X. Q. In Situ X-ray Diffraction Studies of Mixed LiMn$_2$O$_4$−LiNi$_{1/3}$Co$_{1/3}$Mn$_{1/3}$O$_2$ Composite Cathode in Li-Ion Cells During Charge−Discharge Cycling. *J. Power Sources* **2009**, *192*, 652−659.

(14) Yoon, W. S.; Nam, K. W.; Jang, D. H.; Chung, K. Y.; Hanson, J.; Chen, J. M.; Yang, X. Q. The Kinetic Effect on Structural Behavior of Mixed LiMn$_2$O$_4$−LiNi$_{1/3}$Co$_{1/3}$Mn$_{1/3}$O$_2$ Cathode Materials Studied by In Situ Time-resolved X-ray Diffraction Technique. *Electrochem. Commun.* **2012**, *15*, 74−77.

(15) Ito, A.; Li, D. C.; Sato, Y.; Arao, M.; Watanabe, M.; Hatano, M.; Horie, H.; Ohsawa, Y. Cyclic Deterioration and its Improvement for Li-rich Layered Cathode Material Li$[$Ni$_{0.17}$Li$_{0.2}$Co$_{0.07}$Mn$_{0.56}]$O$_2$. *J. Power Sources* **2010**, *195*, 567−573.

(16) Simonin, L.; Colin, J. F.; Ranieri, V.; Canévet, E.; Martin, J. F.; Bourbon, C.; Baehtz, C.; Strobel, P.; Daniela, L.; Patoux, S. In situ Investigations on a Li-rich Mn-Ni Layered Oxide for Li-Ion battery. *J. Mater. Chem.* **2012**, *22*, 11316−11323.

(17) Li, J.; Klöpsch, R.; Stan, M.; Nowak, C. S.; Kunze, M.; Winter, M.; Passerini, S. Synthesis and Electrochemical Performance of the High Voltage Cathode Material Li$[$Li$_{0.2}$Mn$_{0.56}$Ni$_{0.16}$Co$_{0.08}]$O$_2$ with Improved Rate Capability. *J. Power Sources* **2011**, *196*, 4821−4825.

(18) Park, K. S.; Song, C. H.; Stephan, A. M.; Jeong, S. K.; Nahm, K. S.; Oh, S. M.; Kim, Y. G. Influence of Solvents on the Synthesis and Electrochemical Properties of Li$[$Li$_{1/5}$Ni$_{1/10}$Co$_{1/5}$Mn$_{1/2}]$O$_2$ for the Applications in Lithium-ion Batteries. *J. Mater. Sci.* **2006**, *41*, 7628−7635.

(19) Zhao, Y. J.; Zhao, C. S.; Sun, Z. Q.; Feng, H. L. Synthesis and Characterization of Li-rich Cathode Materials Li$[$Li$_{(1/3−x/3)}$Co$_x$Mn$_{(2/3−2x/3)}]$O$_2$ by Modified Pechini Method. *Acta Chim. Sin. (Engl. Ed.)* **2011**, *69*, 117−121.

(20) Hong, Y. S.; Park, Y. J.; Ryu, K. S.; Chang, S. H.; Kim, M. G. Synthesis and Electrochemical Properties of Noncrystalline Li$[$Ni$_x$Li$_{(1−2x)/3}$Mn$_{(2−x)/3}]$O$_2$ Prepared by a Simple Combustion Method. *J. Mater. Chem.* **2004**, *14*, 1424−1429.

(21) Du, K.; Huang, X.; Hu, G. R.; Peng, Z. D. Synthesis and Electrochemical Properties of Li$[$Li$_{0.2}$Ni$_{0.2}$Mn$_{0.6}]$O$_2$ as High Capacity Cathode Material. *Trans. Nonferrous Met. Soc. China* **2012**, *22*, 1201−1208.

(22) Armstrong, A. R.; Holzapfel, M.; Novak, P.; Johnson, C. S.; Kang, S. H. Demonstrating Oxygen Loss and Associated Structural Reorganization in the Lithium Battery Cathode Li$[$Ni$_{0.2}$Li$_{0.2}$Mn$_{0.6}]$O$_2$. *J. Am. Chem. Soc.* **2006**, *128*, 8694−8698.

(23) Yu, L. Y.; Qiu, W. H.; Lian, F.; Liu, W.; Kang, X. L.; Huang, J. Y. Comparative Study of Layered 0.65Li$[$Li$_{1/3}$Mn$_{2/3}]$O$_2$·0.35LiMO$_2$ (M = Co, Ni$_{1/2}$Mn$_{1/2}$, and Ni$_{1/3}$Co$_{1/3}$Mn$_{1/3}$) Cathode Materials. *Mater. Lett.* **2008**, *62*, 3010.

(24) Guo, X. J.; Li, Y. X.; Zheng, M.; Zheng, J. M.; Li, J.; Gong, Z. L.; Yang, Y. Structural and Electrochemical Characterization of xLi$[$Li$_{1/3}$Mn$_{2/3}]$O$_2$·$(1−x)$ Li$[$Ni$_{1/3}$Mn$_{1/3}$Co$_{1/3}]$O$_2$ $(0 ≤ x ≤ 0.9)$ as Cathode Materials for Lithium Ion Batteries. *J. Power Sources* **2008**, *184*, 414.

(25) Johnson, C. S.; Li, N.; Vaughey, J. T.; Hackney, S. A.; Thackeray, M. M. Lithium−Manganese Oxide Electrodes with Layered-Spinel Composite Structures xLi$_2$MnO$_3$·$(1 − x)$Li$_{1+y}$Mn$_{2y}$O$_4$ $(0 < x < 1, 0 ≤ y ≤ 0.33)$ for Lithium Batteries. *Electrochem. Commun.* **2005**, *7*, 528−536.

(26) Shao, H. Y.; Hackney, S. A.; Armstrong, A. R.; Bruce, P. G.; Gitzendanner, R.; Johnson, C. S.; Thackeray, M. M. Structural Characterization of Layered LiMnO$_2$ Electrodes by Electron Diffraction and Lattice Imaging. *J. Electrochem. Soc.* **1999**, *146*, 2404−2412.

(27) Armstrong, A. R.; Paterson, A. J.; Dupre, N.; Grey, C. P.; Bruce, P. G. Structural Evolution of Layered Li$_x$Mn$_y$O$_2$: Combined Neutron, NMR, and Electrochemical Study. *Chem. Mater.* **2007**, *19*, 1016−1023.

(28) Johnson, C. S.; Li, N. C.; Lefief, C.; Vaughey, J. T.; Thackeray, M. M. Synthesis, Characterization and Electrochemistry of Lithium Battery Electrodes: xLi$_2$MnO$_3$·$(1 − x)$LiMn$_{0.333}$Ni$_{0.333}$Co$_{0.333}$O$_2$ $(0 ≤ x ≤ 0.7)$. *Chem. Mater.* **2008**, *20*, 6095−6106.

(29) Wang, D.; Liu, L. M.; Zhao, S. J.; Li, B. H.; Liu, H.; Lang, X. F. β-MnO$_2$ as a Cathode Material for Lithium Ion Batteries from First Principles Calculations. *Phys. Chem. Chem. Phys.* **2013**, *15*, 9075−9083.